Check for updates

AGU ADVANCING EARTH AND SPACE SCIENCE

Water Resources Research

RESEARCH ARTICLE
10.1029/2020WR028377

Effects of Downward Intrusion of Saline Water on Nested Groundwater Flow Systems

Xiaolang Zhang[1,2], Jiu Jimmy Jiao[1], Hailong Li[2,3], Xin Luo[1], and Xingxing Kuang[2,3]

[1]Department of Earth Sciences, University of Hong Kong, Hong Kong, [2]School of Environmental Science and Engineering, Southern University of Science and Technology, Shenzhen, China, [3]Guangdong Provincial Key Laboratory of Soil and Groundwater Pollution Control, Southern University of Science and Technology, Shenzhen, China

Key Points:

- The effects of boundary salinity values ranging from 0 to 200 g/L in the discharge zones on the hierarchal flow systems are quantified
- The local groundwater flow and the internal stagnation points all shift upward with the increase of salinity
- The discharge zone is expanded, and the overall groundwater velocity magnitude of all the flow systems decreases as the salinity increases

Correspondence to:
J. J. Jiao,
jjiao@hku.hk

Citation:
Zhang, X., Jiao, J. J., Li, H., Luo, X., & Kuang, X. (2020). Effects of downward intrusion of saline water on nested groundwater flow systems. *Water Resources Research*, *56*, e2020WR028377. https://doi.org/10.1029/2020WR028377

Received 23 JUL 2020
Accepted 28 SEP 2020
Accepted article online 2 OCT 2020

Abstract Nested groundwater flow systems (NGFS) are commonplace in various hydrogeological environments, including endorheic basins and coastal aquifers. The subsystems of the NGFS can be spatially separated by streamlines around the internal stagnation points. At the discharge zones of the topographic depressions, saline water often emerges due to high evaporation in endorheic drainage basins or the combined effects of evaporation and intermittent seawater submersion in coastal areas. To date, there are limited studies that have considered the impact of local-scale downward migration of saline plumes in the topographic depressions on the NGFS. In this study, the classic NGFS are revisited by considering saline water in their discharge zones. To quantify the effects of salinity in the discharge zones on the NGFS, scenarios of various salinities in the discharge zones are simulated. The displacements of the internal stagnation points are used to quantify the evolution of the NGFS in response to salinity changes in the discharge zones. The results show that, as the salinity in the discharge zones increases, the hydraulic gradient near the discharge zone can be significantly reduced, the internal stagnation points shift upward, and the local groundwater flow systems retreat upward so that their original spaces are replaced by intermediate or regional flow systems. The discharge zone is expanded, and the overall groundwater flow velocity magnitude of the entire system decreases with salinity. This study may shed light on the management of saline wetlands, for example, the control of groundwater salinization, evolution of saline groundwater basins, and seawater intrusion.

1. Introduction

Tóth (1963) was the first to show that the groundwater flow is characterized by hierarchal nested groundwater flow systems (referred to hereafter as NGFS). These systems typically consisted of local, intermediate, and regional groundwater flow systems and are thought to exist in many hydrogeological environments, including endorheic basins (Figure 1a), coastal aquifers (Figure 1b) (Wilson, 2005), hyporheic zones (Boano et al., 2014), and river basins (Zlotnik et al., 2011). Groundwater flow systems mediate a variety of geological, geophysical, and biogeochemical processes in both shallow and deep underground environments (Garven, 1995; Person et al., 1996; Schwartz & Domenico, 1973; Stuyfzand, 1999; Szijártó et al., 2019; Tóth, 1999). Understanding such groundwater flow systems is of great practical relevance to ore mineralization (Garven et al., 1993, 1999; Garven & Freeze, 1984; Raffensperger & Garven, 1995), petroleum migration (Garven, 1989), sediment diagenesis (Lee & Bethke, 1994), heat transfer (Szijártó et al., 2019), hydrochemical patterns (Gupta et al., 2015; Jiang et al., 2014; Stuyfzand, 1999; Wang et al., 2015), etc.

Subsystems of the NGFS are characterized by having different hydraulic and hydrogeochemical patterns. Local flow systems are shallow, small-scale circulations that flow from water table crests to adjacent troughs. Circulations of intermediate flow systems are typically deeper, and their flow lines extend over several water table crests and troughs. Regional flow system extends over the full domain of the aquifer. Solute concentrations and mean groundwater ages increase down gradient, and thus local flow systems are featured by young groundwater and low solute concentration (Jiang et al., 2010). Chemical processes, including dissolution, hydration, hydrolysis, oxidation-reduction reactions, chemical precipitation, ion exchange, and reduction of sulfate are all intensified along the regional groundwater flow path.

Stagnation zones, which are defined as the points where flow velocities equal 0 (Wang et al., 2011), are not only the hydrostatic zones but also trap zones of transported matter or heat (Tóth, 1999). There are two types

©2020. American Geophysical Union. All Rights Reserved.

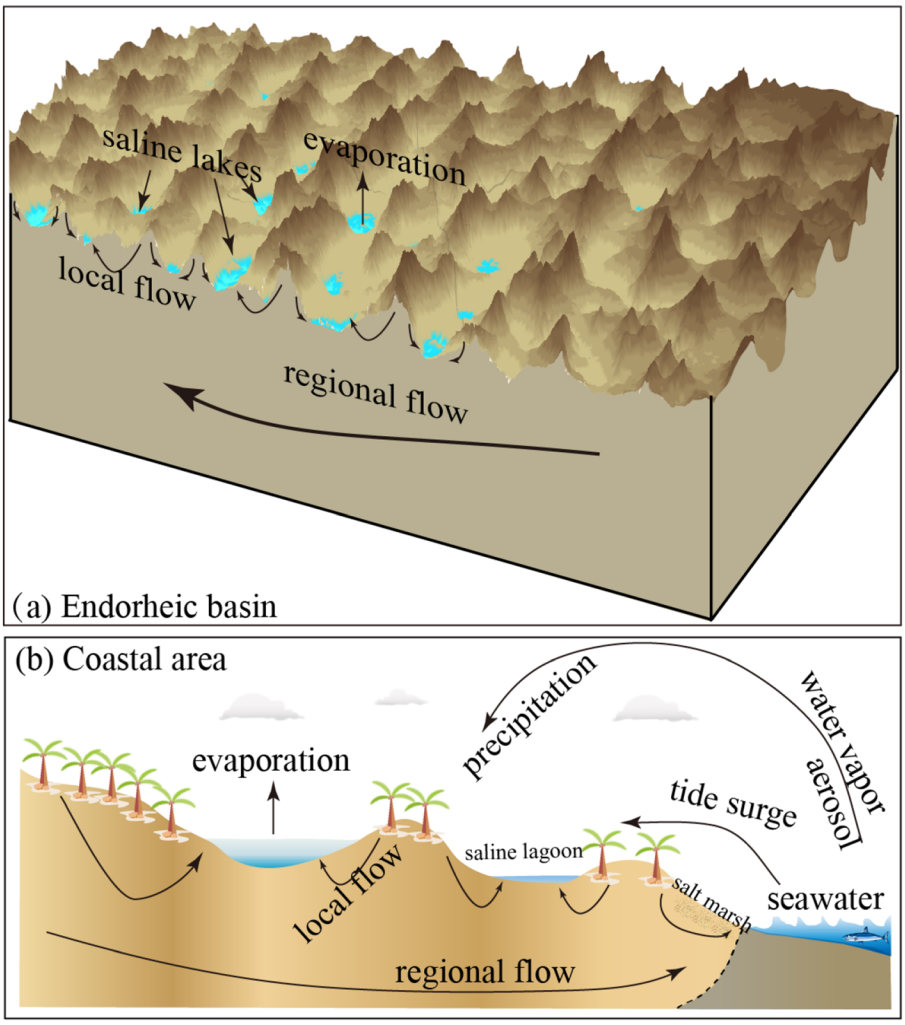

Figure 1. Schematics of saline water impacts on the NGFS in (a) endorheic basin based on the groundwater flow system in the Badain Jaran Desert and (b) coastal area.

of stagnation points: internal and basin bottom (Jiang et al., 2014). After identifying the positions of internal stagnation points, and drawing streamlines around these internal stagnation zones, the local, intermediate, and regional groundwater flow systems can be divided by these streamlines. Thus, the internal stagnation points are extremely useful for distinguishing and identifying these subsystems. In this study, we used the displacements of the internal stagnation points to indicate the change of the NGFS in response to the salinity changes in the discharge zones.

Saline lakes, marshes, lagoons, and wetlands typically form in endorheic basins and coastal areas. About 10% of the Earth's surface is occupied by closed or endorheic drainage basins (Waiser & Robarts, 2009), where surface water bodies are usually saline due to high evaporation. For example, in the Badain Jaran Desert in Inner Mongolia, China, there are over 100 lakes among the mega sand dunes, and most of the lakes are saline, with salinity ranging from 1.2 to 483 g/L (Jiao et al., 2015; Wang & Zhou, 2018). Saline water bodies are also ubiquitous in shallow aquifers (Wang & Jiao, 2012) or lagoons (Santos et al., 2008) in coastal regions due to marine transgression and regression (Han et al., 2011), sea level rise (Gulley et al., 2016), or surge (Jiao & Post, 2019).

The dense saline water may sink and replace the underlying fresh groundwater to reach stability. As a result, the saline water in the surface water body will first modify groundwater flow around the saline water body (Duffy & Al-Hassan, 1988; Fan et al., 1997; Wooding et al., 1997) and then eventually change the entire flow system when the modification propagates upstream. There are numerous studies on downward convection

Table 1
Model Parameter Values and Attributes for the Base Case

Description	Value	Unit	Reference and remarks
Hydraulic conductivity of saturated fresh water	1	m/day	Jiang et al. (2009)
Longitudinal dispersivity	10	m	Giving the local-scale dispersivity to be 0.015 (Fan et al., 1997)
Transverse dispersivity	1	m	Giving transverse/longitudinal dispersivity = 0.1
Molecular diffusion coefficient	8.64×10^{-6}	m^2/day	
Porosity	0.37	—	Typical value for silt
Fresh water density	1,000	kg/m^3	
Fresh water viscosity	86.5	Pa·day	
Maximum salt concentration	200	g/L	
Maximum salt water density	1,140	kg/m^3	Based on Equation 2
Maximum salt water viscosity	105.698	Pa·day	Based on Equation 3

of salt plumes and their impacts on local-scale groundwater flow (Geng & Boufadel, 2015a, 2015b). Interactions between local groundwater flow systems and intermediate or regional systems will probably spread the local hydraulic perturbations to the whole NGFS. However, the hydrodynamics mechanisms of such situations and the effects of downward intrusion of saline water on environments are still unclear.

Saline water bodies in the discharge zones are expected to modify the flow system structure and hydrochemical patterns. Initially, saline water in the discharge zones increases the freshwater-equivalent head of the local groundwater so that the gradients both in local and regional scales are decreased, and consequently the groundwater velocity is reduced. Second, because the groundwater flow rate is reduced, the groundwater will have more time to interact with the aquifer matrix, and thus the groundwater age and solute concentration will increase. Furthermore, the heavier and denser saline water will likely infiltrate into the aquifer and degrade the water quality. Misunderstanding the effects of saline water intrusion in the topographic depressions may lead to overestimating the groundwater renewal capacity and underestimating the hydrochemical changes.

The overall objective of this study was to explore the role of density-dependent flow on the NGFS due to downward intrusion of saline water in the discharge zones. The theoretical model of regional groundwater flow developed by Tóth (1963) was modified to explore the effects of downward intrusion of saline water. At first, a steady state groundwater flow model without solute transport (zero salinity) was conducted to determine the discharge and recharge zones of the domain. Then different density-dependent flow models (Table 1) were developed by applying a *Dirichlet* salinity boundary condition ranging from 10 to 200 g/L along the discharge boundaries of the steady state, no-solute model. In order to explore the effects of dispersivity, hydraulic conductivity, model domain scale, and local and regional flow system scale, six test cases (Table 2) were compared with the base case. Finally, the implications of the modification of the NGFS by the salinity increase in the discharge zones were discussed.

Table 2
Simulated Test Cases With Model Parameter Values

Cases	α_L (m)	K (m/day)	L (m)	Z_0 (m)	A (m)	b (m^{-1})	tanα (–)
Base case	10	1	6,000	1,000	15	$2\pi/1500$	0.02
Case 1	5.88	1	6,000	1,000	15	$2\pi/1500$	0.02
Case 2	50	1	6,000	1,000	15	$2\pi/1500$	0.02
Case 3	10	10	6,000	1,000	15	$2\pi/1500$	0.02
Case 4	10	1	3,000	500	7.5	$4\pi/1500$	0.02
Case 5	10	1	6,000	1,000	22.5	$2\pi/1500$	0.02
Case 6	10	1	6,000	1,000	15	$2\pi/1500$	0.03

Note. For all cases, 12 different salinities (10, 20, 35, 40, 60, 80, 90, 100, 110, 120, 150, and 200 g/L) are specified on the discharge zones of the base case; the transverse dispersivity is always set to be 0.1 times the longitudinal dispersivity. The values of all other parameters that are not listed in Table 2 are the same as those of the base case.

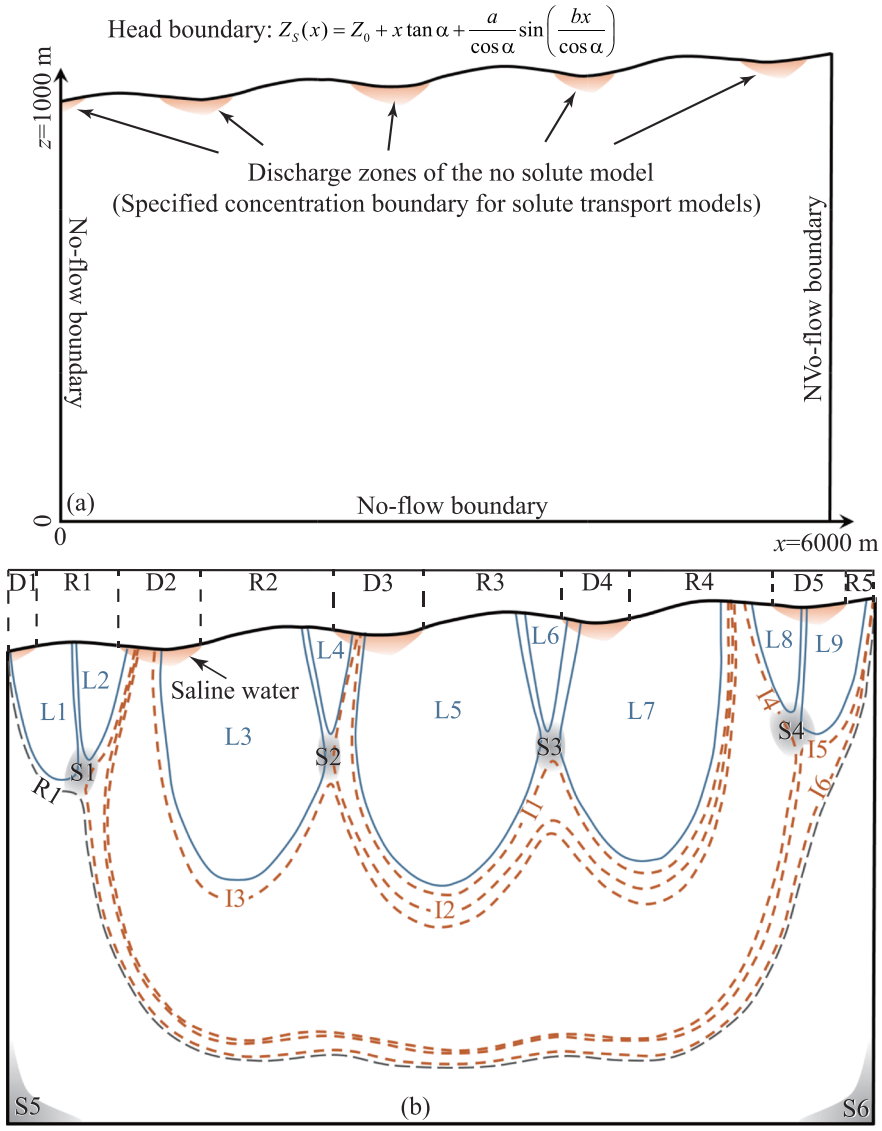

Figure 2. Model setup and simulation results of the steady state no-solute transport model (zero salinity). (a) Boundary conditions; (b) the NGFS based on the numerical simulation results of no-solute transport model. S1, S2, ..., S6 denote the stagnation points. There are nine local flow systems (L1, L2, ..., L9). Intermediate Flow Systems IF1, IF2, and IF3 are divided by Streamlines I1 and I2, I3 and I4, and I5 and I6, respectively. The domain below Streamline R1 is occupied by regional flow system. The orange areas near the water table indicate the high-salinity zones. D and R denote discharge and recharge zones, respectively.

2. Numerical Methods

Numerical modeling was performed using HydroGeoSphere (Brunner & Simmons, 2012), in which the saturated subsurface flow is calculated by Darcy's law. The advection-dispersion-diffusion equation is solved for salt transport. Details concerning the theory, governing equations, and numerical solution techniques of HydroGeoSphere are given in Therrien et al. (2006).

2.1. Defining the Conceptual Model

The conceptual model was framed from the classic Tóth (1963) model. The modeling domain was a two-dimensional cross section, about 6,000 m wide and 1,000 m high (Figure 2a). Following Tóth (1963), the ground surface of the synthetic basin was defined by the following equation:

$$Z_S(x) = Z_0 + x\tan\alpha + \frac{a}{\cos\alpha}\sin\left(\frac{bx}{\cos\alpha}\right) \quad (1)$$

where Z_0 = 1,000 m, $x \in (0, 6{,}000)$, $\tan\alpha = 0.02$, a = 15 m, and $b = 2\pi/1{,}500\ \mathrm{m}^{-1}$ (Figure 2a). In this equation, $\tan\alpha$ represents the regional hydraulic gradient; $a/\cos\alpha$ represents the amplitude of local topographic fluctuations, and the local undulation has a wavelength of 1,500 m; thus, the local gradient is 0.02. The basin bottom was set at $z = 0$. The water table was assumed to mimic the ground surface, and thus the water table had the same function as Equation 1. The side and bottom boundaries were set to be impermeable.

The model domain was horizontally discretized at a 7.5 m resolution, with 100 vertical layers of equal thickness. The grid had 80,901 nodes and 80,000 elements in the *x*-*z* plane. In order to determine whether a higher discretization would affect the simulation results, we ran a test with increased horizontal discretization (5 m resolution) and 120 vertical layers. The higher resolution produced negligible differences in boundary salinity value distribution and locations of stagnation points, which indicated that the initial resolution was appropriate for capturing the dynamics of salt and water flow.

2.2. Identifying the Flow Patterns of a No-Solute Transport Model

Steady state groundwater flow without solute transport was simulated to identify the discharge and recharge zones of the domain, the original positions of the stagnation points, and the hierarchy of the NGFS (Figure 2b). The discharge and recharge zones were determined based on groundwater flow direction in the upper surface boundary. After identifying the positions of S1 to S4, and drawing the 9 local streamlines, 6 intermediate streamlines and 1 regional streamline around the four stagnation zones, the local, intermediate, and regional flow systems can be divided using the 16 different streamlines. As shown in Figure 2b, there are nine local flow systems (from L1 through L9). Intermediate Flow Systems IF1, IF2, and IF3 are divided by streamlines I1 and I2, I3 and I4, and I5 and I6, respectively. The domain below streamline R1 is occupied by the regional flow system (RF). D and R denote discharge and recharge zones, respectively.

2.3. Defining Density-Dependent Flow Properties

In the advection-dispersion-diffusion equation, the solute transport variable is salinity, c ($\mathrm{M/L^3}$) (Graf & Therrien, 2005). The fluid density and viscosity are both as functions of changes in the salinity. Most density-dependent groundwater flow simulations are based on a linear equation that relates the salinity to the fluid density:

$$\rho = \rho_0 + \gamma c \quad (2)$$

where ρ ($\mathrm{M/L^3}$) and ρ_0 ($\mathrm{M/L^3}$) are the fluid densities of saline water and fresh water, respectively. The slope of the linear equation γ (–) ranges between 0.64 and 0.75, when this equation is applied to different saline waters (Kohfahl et al., 2015), and a typical value of 0.71 was used in this study. Then the density ratio $\beta = \rho/\rho_0$ equals $1+\zeta c$ (–), where the constant ζ is 7.1×10^{-4} (–). Most of the lakes in the Badain Jaran Desert have salinities below 200 g/L (Rioual et al., 2013). Thus, the simulated maximum salinity in this study was 200 g/L.

The viscosity of saline water also increases with salinity. Here the exponential relation of dynamic viscosity and salinity was adopted from the observed empirical relation of Dead Sea brines (Weisbrod et al., 2016).

$$\mu_r = \mu_0 \cdot e^{0.001 \cdot c} \quad (3)$$

where μ_r (M/[L T]) and μ_0 (M/[L T]) are the dynamic viscosities of saline water and fresh water, respectively.

2.4. Setup of the Base Case and Test Cases

As shown in Figure 2a, discharge occurs in the topographic depressions and salt accumulation usually takes places due to evaporation or/and saline water submersion. The orange areas (Figure 2a) near the water table indicate the high-salinity zone due to downward intrusion of saline water. For the base case (Table 1), a *Dirichlet* salinity boundary condition was applied at the surface of the discharge zones. Twelve different boundary salinities (10, 20, 35, 40, 60, 80, 90, 100, 110, 120, 150, and 200 g/L) were used to investigate their effects on the displacements of the internal stagnation points and the evolution of the NGFS. Each of the models was run until a steady state was achieved (the time to reach a steady state was usually less than

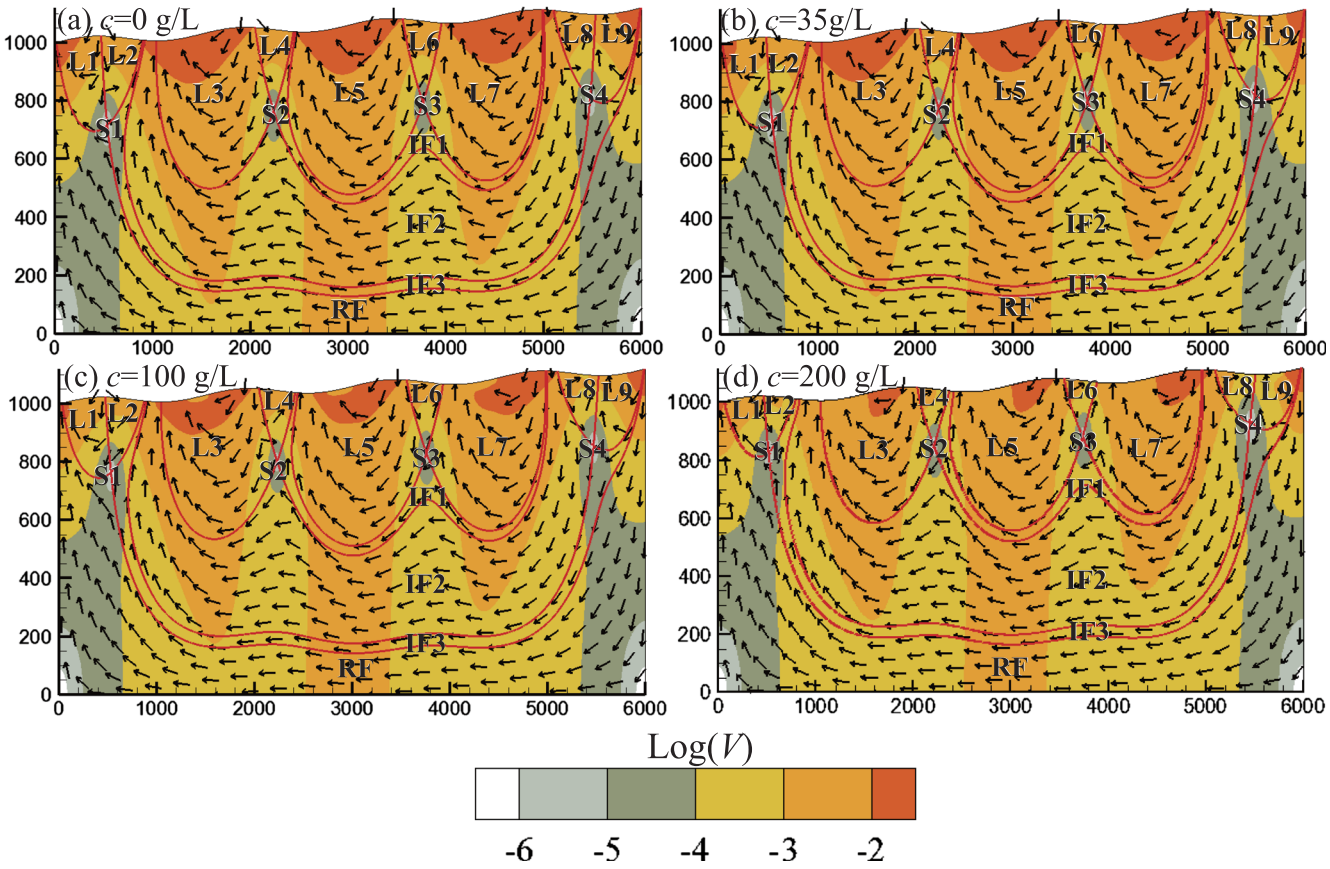

Figure 3. Darcy velocity magnitude Log(*V*) (the unit of |*V*| is m/day) contours (in color bands), streamlines (red solid lines), and velocity direction (black arrows with uniform length) of the base case resulting from different boundary salinities in the discharge zones.

1,000 years, and after that the salinity contours showed no change). In order to explore the effects of dispersivity, hydraulic conductivity, and scale issues, Cases 1 to 6 were designed for sensitivity analysis of these factors (Table 2). In each case, the above mentioned 12 different boundary salinities were performed in terms of the *Dirichlet* boundary condition.

3. Effects of Downward Intrusion of Saline Water on the Flow Field

The effects of downward intrusion of saline water on the flow field are shown in Figure 3. The velocity magnitude of the domain, especailly at the local scale, was reduced due to downward intrusion of saline water. According to the general Darcy's law (Boufadel, 2000), the groundwater velocity in saline environments is

$$\vec{v} = (v_x, v_z) = -\delta K_0\left(\frac{\partial \psi_0}{\partial x}, \frac{\partial \psi_0}{\partial z} + \beta\right) = -\delta K_0\left(\frac{\partial \psi_0}{\partial x}, \frac{\partial \psi_0}{\partial z} + 1 + \zeta c\right) \quad (4)$$

where ψ_0 (L) is the equivalent freshwater pressure head. $\delta = \mu_0/\mu$ (–);

$$K_0 = \kappa\rho_0 g/\mu_0 \quad (5)$$

is the hydraulic conductivity of saturated fresh water, where κ is the intrisic permeability (L^2), and g is the gravitational acceleration (L/T^2).

Changes of viscosity and density both play a role in decreasing the vertical velocity magnitude. In freshwater environments, $v_z = -K_0\left(\frac{\partial \psi_0}{\partial z} + 1\right)$, but in saline environments, the hydraulic gradient is reduced by ζc, and the hydraulic conductivity is also reduced to δK_0. Because $\delta = 1/e^{0.001 \cdot c} < 1$, v_x is also reduced by a factor of

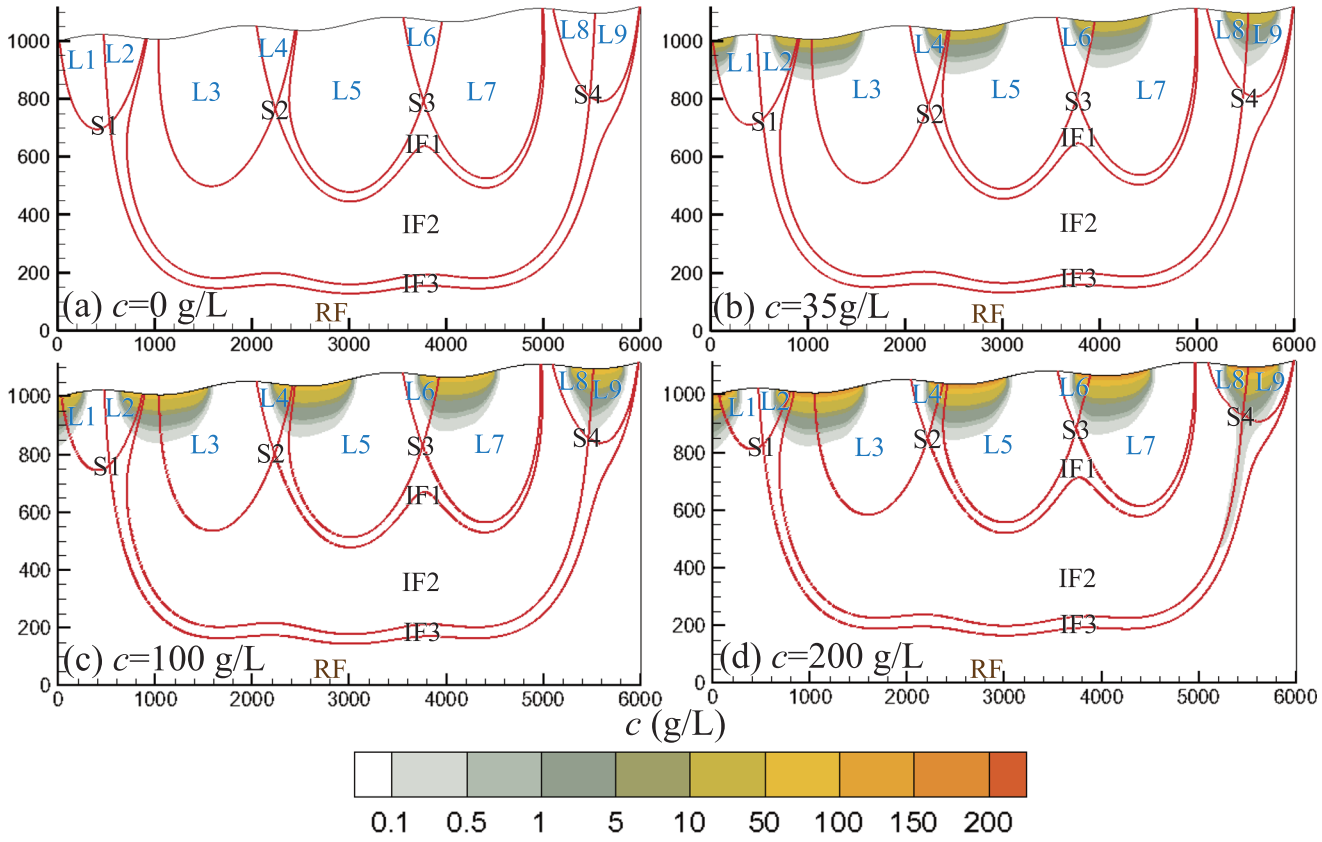

Figure 4. Distributions of salinity of the base case resulting from different boundary salinities in the discharge zones; (a) c = 0 g/L; (b) c = 35 g/L; (c) c = 100 g/L; and (d) c = 200 g/L.

δ during the downward intrusion of saline water. Given that c = 200 g/L and δ = 0.82, the density gradient ζc will be 0.14. Under these conditions the hydraulic gradient can be reduced by 0.14, 7 times higher than the local and regional hydraulic gradient of 0.02. This density gradient is comparable to a topographic gradient classified as high relief (>0.1) according to Gleeson and Manning (2008).

4. Saline Water Transport

The effects of downward intrusion of saline water on the saline plume distribution are shown in Figure 4. Although the groundwater movement in the discharge zone is upward, salt can still transport downward into the aquifer by both dispersion effects (mechanical dispersion and molecular diffusion). Our modeling shows that as the boundary salinity values increase at the discharge zones of the NGFS, the saline water plumes move farther downward (Figures 4a–4d). Although the dominant direction of salt transport is downward, horizontal migration of salt can become more significant as the penetration depth increaes due to intermediate and regional advection. Once the saline water plumes reach the intermediate or regional flow systems (Figure 4d), horizontal migration of the saline water plume driven by advection becomes significant, and finally saline water migrates to the lowest discharge zone. As the saline plume moves down gradient, the plume will expand and dissipate via dispersion and diffusion.

5. Shifts of Stagnation Points and Local Flow Penetration Depths

Because the locations of Internal Stagnation Points S1–S4 can be used to pin the NGFS, it is possible to investigate the evolution of NGFS via shifts of stagnation points due to different boundary salinities. Compared with their original positions in Figure 4a, the stagnation points and penetration depths of the local flow systems in Figures 4b–4d all shift upward. Areas of the local flow systems L1–L9 all shrink in various degrees

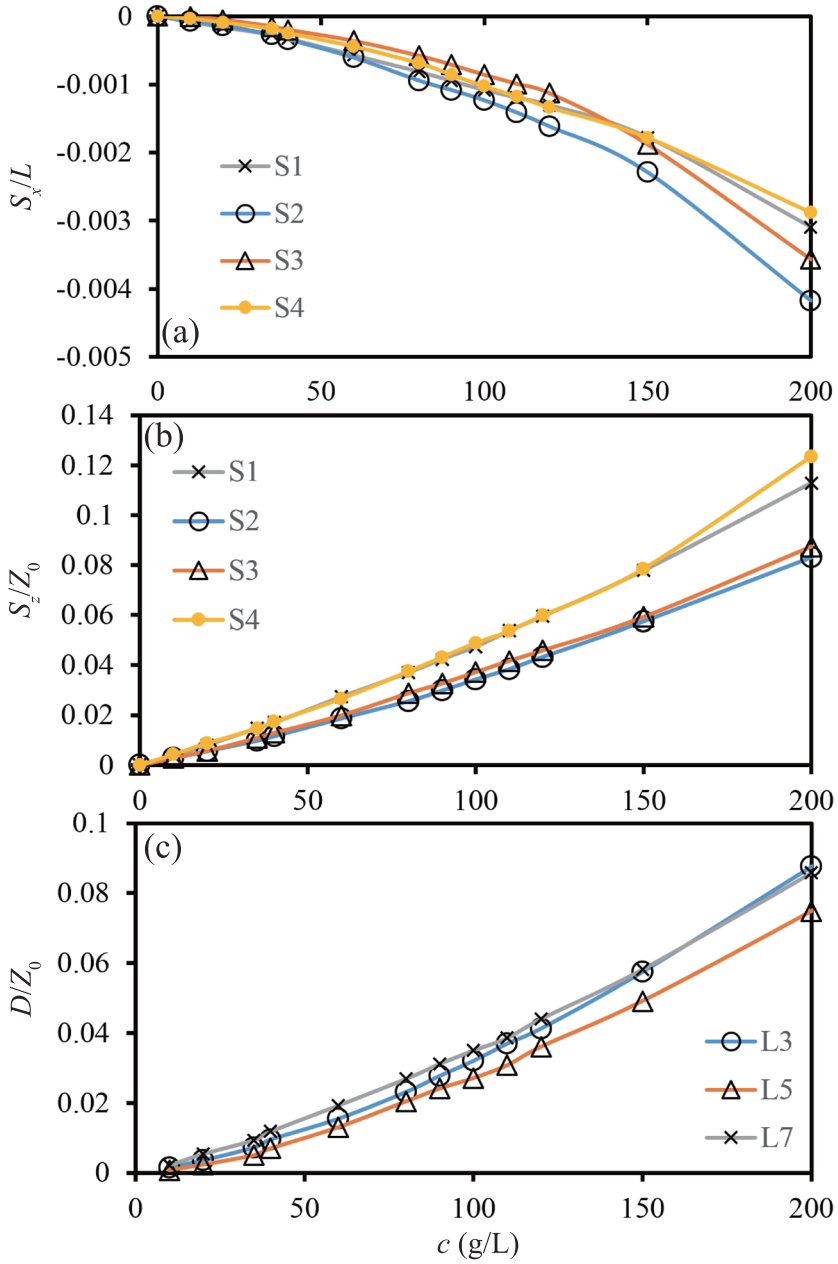

Figure 5. Changes of the normalized displacements of the locations of the four stagnation points (a) S_x/L in the x direction, (b) S_z/Z_0 in the z direction of the base case with the boundary salinities (L = 6,000 m and Z_0 = 1,000 m). In (c) changes of normalized penetration depth D/Z_0 of the three local flow systems with boundary salinity values are shown. The four Internal Stagnation Points S1, S2, S3, and S4 and the three Local Flow Systems L3, L5, and L7 are shown in Figure 2b.

with the increase of boundary salinity. The change of intermediate flow systems is also noteworthy. Compared with Figure 4a, the area of Intermediate Flow Systems IF1 and IF3 remain nearly constant in Figures 4b–4d; whereas the area of Intermediate Flow System IF2 expands;

To better illustrate how the locations of the stagnation points change with boundary salinity values, variations of normalized displacement of the four stagnation points in the x direction (expressed as S_x/L) with salinity are shown in Figure 5a, and those in the z direction (expressed as S_z/Z_0) are shown in Figure 5b. We found that the four stagnation points all shift leftward (S_x/L becomes more negative as shown in

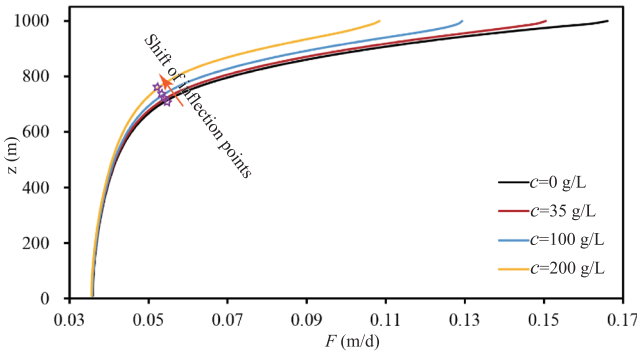

Figure 6. Changes of flushing intensity (F) (m/day) with depth of the base case for four different boundary salinities in the discharge zones.

Figure 5a) and upward (S_z/Z_0 becomes more positive, as shown in Figure 5b). The vertical shift is more significant than the horizontal one.

Variations of normalized penetration depth (expressed as D/Z_0, where D is the lowest location of the local flow system) of three local flow systems (L3, L5, and L7) with the boundary salinity values are shown in Figure 5c. The curves of normalized penetration depth versus the boundary salinity value follow the same pattern as those of vertical displacements of the stagnation points (Figure 5b). This shows that the vertical shift of the stagnation points reflects the transformation of the NGFS.

6. Flushing Intensity

Flushing can be used to measure velocity damping resulting from the increase in boundary salinity values in the discharge zones. Zlotnik et al. (2011) introduced the parameter of flushing (F) (L/T) to quantitatively measure the flushing intensity over the entire domain. In their expression, flushing is the velocity magnitude over a horizontal line at elevation z:

$$\mathrm{F}(z) = \frac{1}{L}\int_0^L |V(x,\, z)|dx = \frac{1}{L}\int_0^L \left[V_x^2(x,\, z) + V_z^2(x,\, z)\right]^{1/2} dx \tag{6}$$

Since their domain geometry was a rectangle, it was convenient to solve the average velocity mathematically over the z plane. In this study, topographic undulations were considered in the numerical model. To simplify the calculation, the flushing was calculated as the averaged velocity over each model layer, and z value is the vertical coordinate of the leftmost node of each layer.

The modeling results are shown in Figure 6. The flushing intensity generally increases with z. Each flushing intensity curve $F(z)$ displays roughly two quasi-linear segments separated by the inflection points (Figure 6). The substantial change near the inflection points is related to the depth where the effect of the local systems vanishes (Zlotnik et al., 2011). This depth is actually the penetration depth of the local flow systems. Beneath this depth, the flow systems are largely driven by regional head gradients, and the undulations of local surface topography become less important. The inflection points of these curves shift upward as boundary salinity values increase from 0 to 200 g/L. This also indicates that the local flow systems retreat upward.

7. Recharge and Discharge

The recharge and discharge rates are important for the circulation patterns and renewal of the groundwater systems. The recharge and discharge rates are shown in Figure 7. Recharge occurs in local or regional topographic highs, and discharge occurs in the topographic depressions. Hinge lines are used to indicate the boundaries between recharge and discharge zones. In Figure 7, hinge lines (vertical black dashed lines) for $c = 0$ g/L are shown. The locations of discharge and recharge zones are significantly affected by boundary salinity values, but they are unaffected by the decrease in hydraulic conductivity with depth (Jiang et al., 2009). The hinge lines shift to higher elevations as the boundary salinity increases (Figures 7a and 7b). Compared to the situation when $c = 0$ g/L, the discharge rate is significantly reduced by saline water boundary conditions. The discharge areas have to be expanded to provide a new water outlet due to the increase of freshwater-equivalent head in the discharge zones. Thus, the recharge areas and the recharge rates are reduced accordingly. It is noteworthy that two discharge areas occur at the two sides of the original recharge zones. In these newly expanded discharge areas, spring and seepage zones are likely to emerge around the topographic depression. Field observations of springs were reported in Duffy and Al-Hassan (1988), who illustrated that springs emerged along the edge region of the saline water based on their simulated results and field observations. Such springs were also found along the shores of the Badain Jaran brine lakes (Wang & Zhou, 2018).

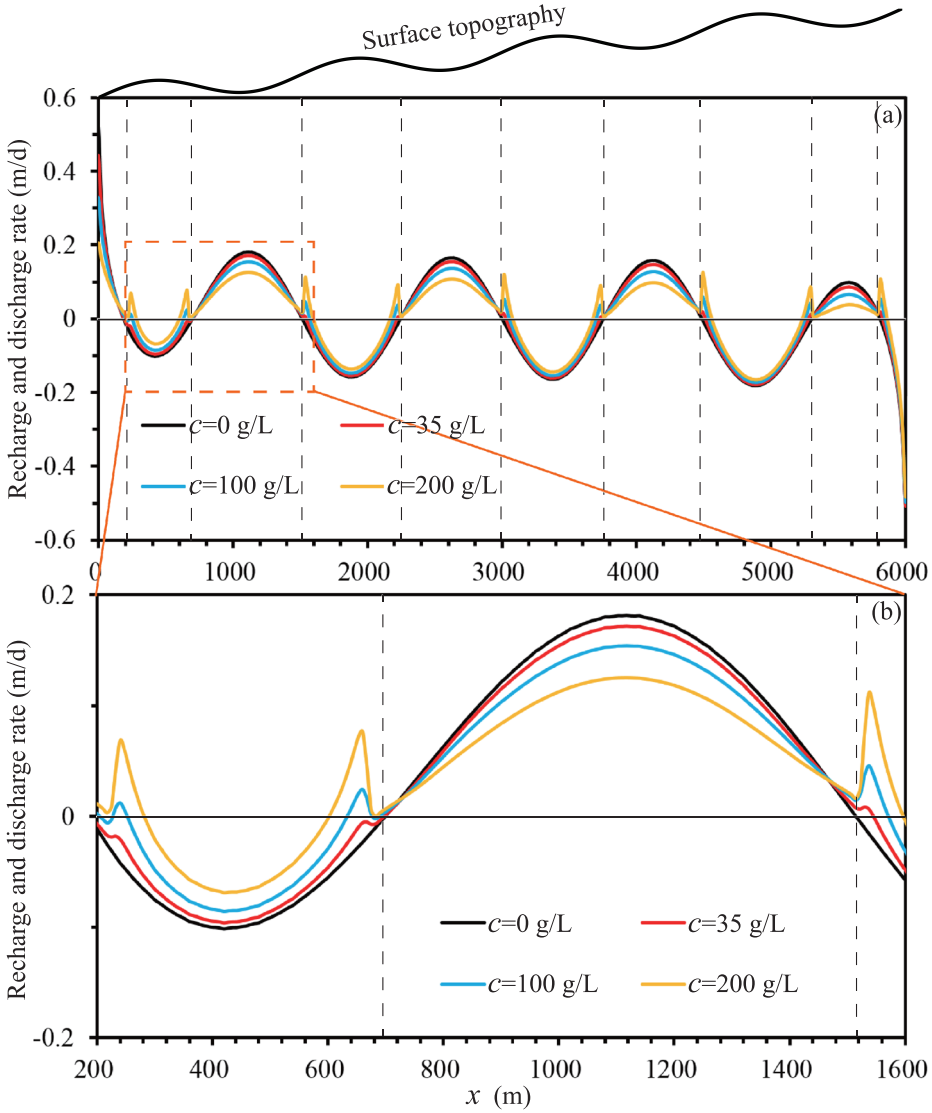

Figure 7. Recharge (negative) or discharge (positive) rates (m/day) on the upper boundary of the domain of the base case. (b) Is the locally enlarged drawing of (a). The black dashed lines indicate the hinge lines that separate discharge and recharge zones for $c = 0$ g/L.

8. Sensitivity Studies

Sensitivity analyses were conducted to investigate the effects of important model parameters on the displacement of the internal stagnation points and thus on the evolution the NGFS (Table 2). The normalized vertical displacements of stagnation points of the tested cases were compared with the base case (Figures 8a, 8b, 9a, 9b, 10a, and 10b). The evolution routes of the four stagnation points of the test cases are shown in Figures 8c, 9c, and 10c. The coordinates of the evolution routes are nondimensional and are normalized to the domain length L in the x direction and the domain height Z_0 in the z direction.

8.1. Dispersivity

Two cases were examined to investigate the effects of dispersivity (see Cases 1 and 2 in Table 2). For Case 1, longitudinal and transverse dispersivities are decreased to 0.59 times the base case to ensure that the grid Peclet number is less than 2 (Diersch & Kolditz, 2002), or equivalently

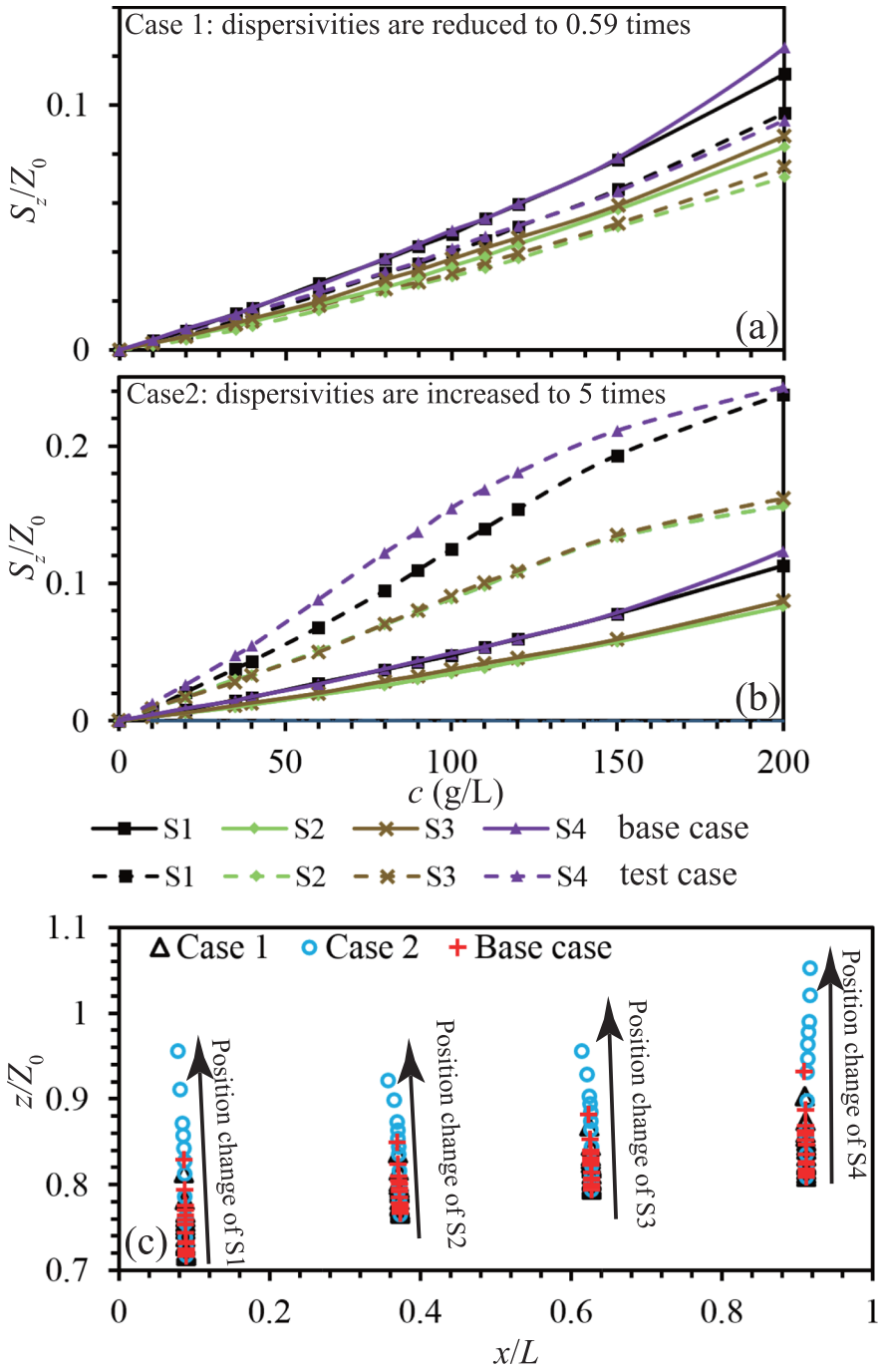

Figure 8. Normalized displacements of four internal stagnation points for (a) Case 1 and (b) Case 2 defined in Table 2; (c) the position displacements of the four Internal Stagnation Points S1, S2, S3, and S4 for the base case, Cases 1 and 2.

$$\alpha_l < d/2 \tag{7}$$

where d (L) is the discretization mesh size, and α_L (L) is the longitudinal dispersivity value; for Case 2, longitudinal and transverse dispersivities are increased by a factor of 5 with respect to the base case;

The vertical displacements of the internal stagnation points in response to changes of dispersivity are non-linear. From Case 1 to the base case, then to Case 2, the dispersivity increases and the vertical displacements of the internal stagnation points also increase (Figures 8a and 8c). This indicates that the salt plume in the

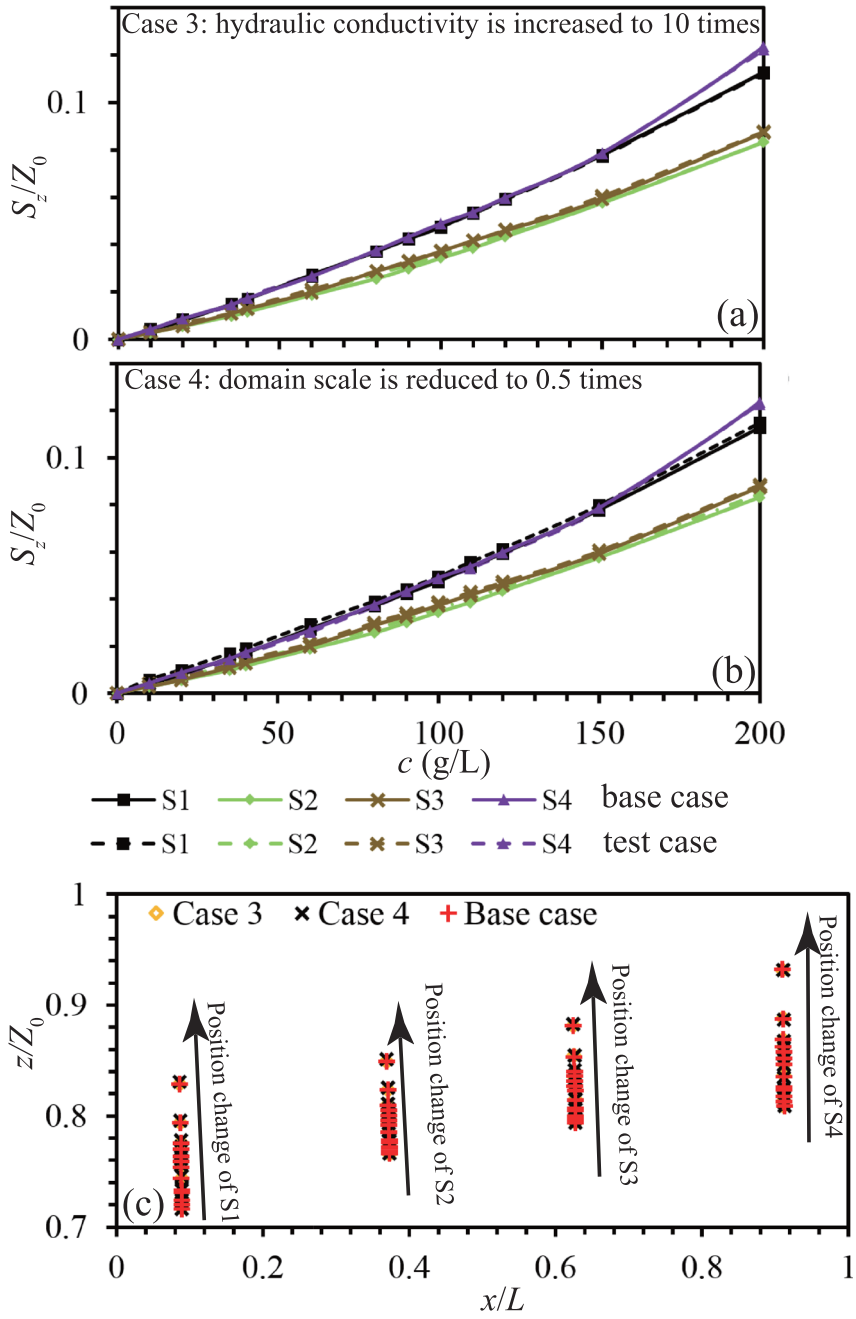

Figure 9. Normalized displacements of stagnation points for (a) Case 3 and (b) Case 4 defined in Table 2; (c) the position displacements of the four Internal Stagnation Points S1, S2, S3, and S4 for the base case, Cases 3 and 4.

three cases is dominated by dispersive transport. The discrepancy between S_z/Z_0 of the three cases is not proportional to the change of dispersivity. In Case 1, the dispersivities are reduced to about 0.59 times the base case, whereas the S_z/Z_0 was about 0.6 to 0.8 times the base case. In Case 2, the dispersivities increased by a factor of 5, and S_z/Z_0 values were about twice those of the base case. A comparison of the base case with Cases 1 and 2 shows that increased dispersion enhances the downward intrusion of saline water and pushes the stagnation points upward (Figure 8c). In Case 1 and the base case, the normalized vertical displacement S_z/L generally increases nearly linearly with increasing salinity (Figure 8a). Nevertheless, at high salinity, the nonlinearity increases, and the slopes of these curves also increase. In Case 2, the curves in Figure 8b present two segments. The slopes of the curves change from steep to gentle.

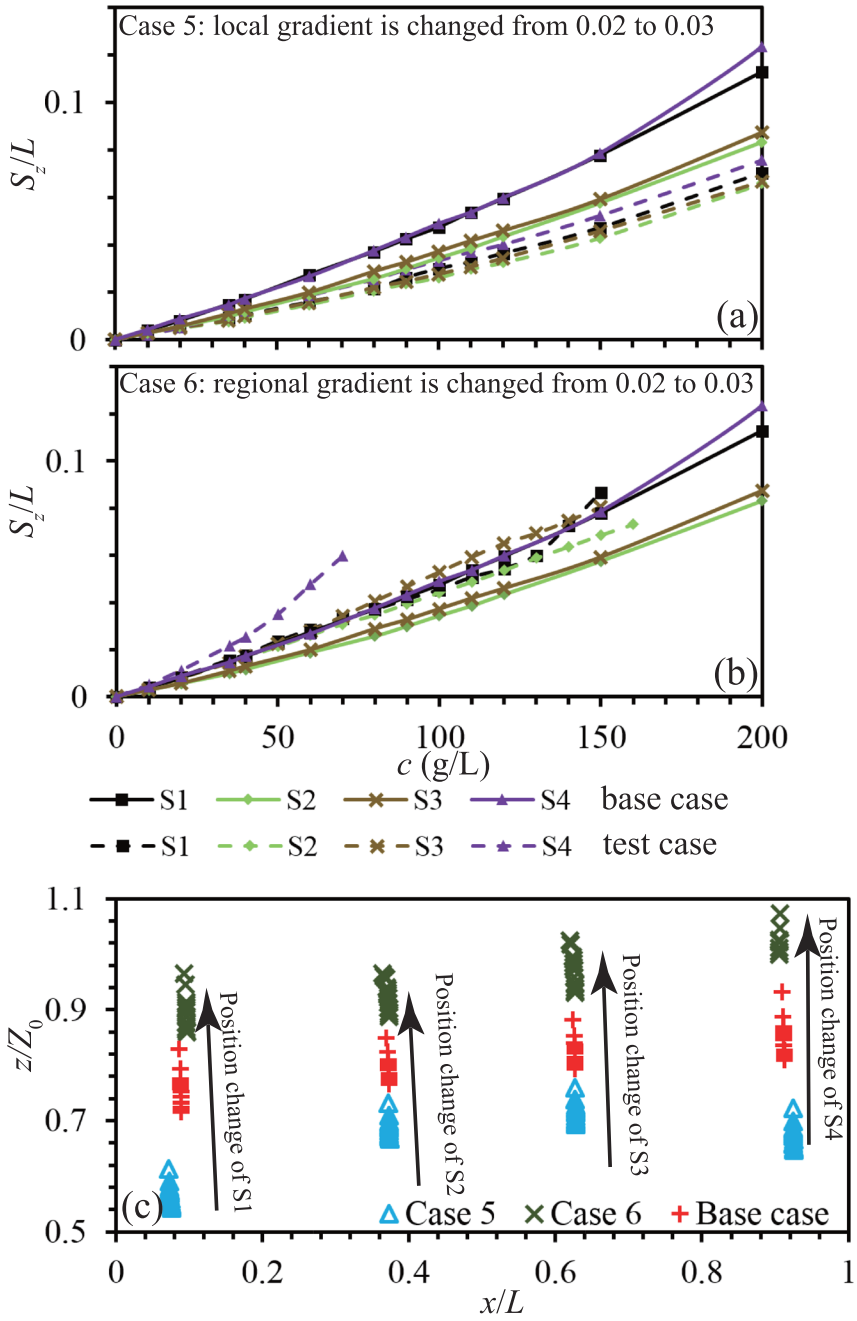

Figure 10. Normalized displacements of stagnation points for (a) Case 5 and (b) Case 6 defined in Table 2; (c) the position displacements of the four Internal Stagnation Points S1, S2, S3, and S4 for the base case, Cases 5 and 6.

8.2. Hydraulic Conductivity and Domain Scale

For Case 3, the hydraulic conductivity is increased to 10 times that of the base case, and for Case 4, the scale of the modeling domain is reduced by a factor of 2 with respect to the base case.

As shown in Figures 9a and 9c, the change of hydraulic conductivity leads to no discrepancy between the base case and Case 3. In homogenous aquifers, the positions of the internal stagnation points are mainly determined by the topographic undulations. Thus, the positions of the internal stagnation points when $c = 0$ g/L and $K = 10$ m/day are the same as those when $c = 0$ g/L and $K = 1$ m/day. As shown in

Equation 4, an increase of hydraulic conductivity leads to no change in δ and ζ. Thus, as the salinity increases, the evolution routes of the four stagnation points of Case 3 and those of the base case are essentially coincident (Figure 9c).

Likewise, when the modeling domain is reduced (halved both in horizontal and vertical directions, Case 5), the vertical displacements of the four internal stagnation points with respect to the base case are almost equivalent (Figure 9b). According to Equation 4, the change of domain scale has no impact on the modification of the hydraulic gradient, and thus the evolution routes of the four stagnation points remain the same (Figure 9c).

8.3. Scale Effect of Subsystems

In the base case, the topographic undulations are referred to as the classic *Tóth* model. The scale of subsystems may affect the evolution of the NGFS and thus is considered further under different simulation scenarios. The scale of subsystems varies with the local and regional gradients. Thus, two cases of different topographic settings are investigated in Cases 5 and 6 (Table 2). For Case 5, the local gradient is increased from 0.02 to 0.03; and for Case 6, the regional gradient is increased from 0.02 to 0.03.

Cases 5 and 6 were designed to analyze the scale effects of subsystems. In Case 4, when the local hydraulic gradient is strengthened, the penetration depth of local flow cells is increased, the local flow systems are enlarged, and the positions of the four stagnation points S1–S4 are deeper than those of the base case (Figure 10a). Compared with the base case, the significant feature of Case 5 is that the vertical displacements of the stagnation points are smaller (Figure 10c). This is because when the local gradient is increased, the recharge rate and thus the resistance forces to downward intrusion of saline water are strengthened. In Case 6, when the regional hydraulic gradient is increased, the penetration depth of the local flow is reduced, and the intermediate and regional flow systems are expanded, while the scale of local flow systems is reduced and the positions of the four stagnation points are higher than those of the base case (Figure 10b). The most striking difference between the base case and Case 6 is that as the salinity increases, the four internal stagnation points keep moving upward as the salinity increases and finally disappear as the boundary salinity increases. When c is greater than 80 g/L, S4 reaches up to the land surface and disappears; when c is greater than 150 g/L, S1, S2, and S3 disappear (Figure 10b). Finally, the local flow systems of L2 and L8 are replaced by Intermediate Flow System IF2, whereas L4 and L6 are replaced by adjacent local flow systems. In addition, the slopes of the curves of S1 and S4 become steeper with the increases in the boundary salinity.

To summarize, the dispersivity, as well as the local and regional gradients, all have prominent effects on the downward intrusion process of saline water and thus on the evolution of the NGFS. This shows that the changes of domain scale and hydraulic conductivity have little effect on the evolution of the NGFS.

9. Implications

The main findings of this study show that after downward intrusion of saline water occurs in the discharge zones of the NGFS, the original short local flow lines are replaced by longer intermediate or regional flow lines. The velocity magnitude is also reduced. These results suggest that the salinity-affected flow systems have weaker renewal capacities.

This study has improved our understanding of how the endorheic groundwater flow systems evolve below saline lakes such as those in the Badain Jaran Desert (Figure 1a). These paleolakes are believed to have been fresh between 30,000 and 20,000 years before the present when the climate was more humid than it is now (Wang et al., 2016; Yang, 2000). When lakes in the desert evolve from fresh to saline states under changing climate conditions, the density effect will modulate the evolution of groundwater flow systems, as the saline lake water intrudes into the lake bed and the groundwater velocity is reduced. Local flow systems with these lakes as the discharge zones will shrink upward, and the space that was previously occupied by local groundwater flow systems will be replaced by intermediate or regional flow systems.

Another analog is groundwater salinization due to intensive phreatic evaporation in the topographic depressions. As the salinization process continues, the groundwater salinity keeps increasing, and the ambient groundwater flow systems can be modified due to migration of saline plumes in the evaporating zones. The local hydraulic perturbation caused by an increase of freshwater-equivalent head and a decrease of

hydraulic conductivity in the salnization zone will finally spread out to the NGFS of the whole groundwater basin. This knowledge can help explain the consequence of groundwater salinization in modifying the groundwater flow systems.

For coastal aquifers, inland water discharge to the sea includes both local and farther regional flow cells (Figure 1b) (Wilson, 2005). Seawater can submerge the coastal depressions because of tide surges or marine transgressions and regressions. Saltwater can intrude into the coastal aquifer via saline estuaries, canals, or lagoons and degrade the shallow fresh groundwater resources. The groundwater flow velocity of the whole system will certainly be reduced as the saltwater intrudes downward. Werner et al. (2013) pointed out that any reduction in the inland water flux would trigger seawater intrusion. The coastal freshwater-saltwater interface will shift inland, and the deep fresh water will also be degraded.

10. Conclusions

Saline water is ubiquitous in endorheic wetlands and coastal areas, favoring density-dependent flow development in these environments. The downward intrusion of salt plumes modulates local-scale groundwater flow, and local hydraulic perturbation propagates to the other subsystems of the NGFS. By adding a specified salinity boundary condition in the discharge zones of the classic *Tóth* model, density effects on the evolution of NGFS were numerically analyzed. The main findings are as follows.

1. The influx of saline water into the NGFS leads mainly to changes in the freshwater-equivalent head and hydraulic conductivity.
2. Local flow systems retreat upward, and the velocity magnitude is reduced with the increase of the boundary salinity in the discharge zones.
3. Internal stagnation points and the NGFS are sensitive to the changes of dispersivity, as well as local and regional gradients, but are insensitive to the changes of hydraulic conductivity and domain scale. When the dispersivity increases, the displacements of the internal stagnation points are also intensified. If the local hydraulic gradient is reduced or the regional gradient is increased, the penetration depth of the local groundwater flow systems becomes shallower. Thus, this type of local groundwater flow system is more easily replaced by intermediate or regional groundwater flow systems as saline water occurs in the discharge zones.

The above findings are helpful in understanding the evolutions of the NGFS with progressively increasing salinity in their discharge zones. They may also contribute to better management and control of saline wetlands in endorheic basins and coastal aquifers.

Data Availability Statement

The input files and output results of the numerical models are available online (http://doi.org/10.5281/zenodo.3950867).

Acknowledgments

This study was supported by grants from National Natural Science Foundation of China (No. 41572208 and 91747204) and the Research Grants Council of Hong Kong (HKU 17304815). The Associate Editor and three anonymous reviewers are thanked for their fruitful comments on the original manuscript.

References

Boano, F., Harvey, J. W., Marion, A., Packman, A. I., Revelli, R., Ridolfi, L., & Wörman, A. (2014). Hyporheic flow and transport processes: Mechanisms, models, and biogeochemical implications. *Reviews of Geophysics*, *52*, 603–679. https://doi.org/10.1002/2012RG000417

Boufadel, M. C. (2000). A mechanistic study of nonlinear solute transport in a groundwater–surface water system under steady state and transient hydraulic conditions. *Water Resources Research*, *36*(9), 2549–2565. https://doi.org/10.1029/2000WR900159

Brunner, P., & Simmons, C. T. (2012). HydroGeoSphere: A fully integrated, physically based hydrological model. *Groundwater*, *50*(2), 170–176. https://doi.org/10.1111/j.1745-6584.2011.00882.x

Diersch, H.-J. G., & Kolditz, O. (2002). Variable-density flow and transport in porous media: Approaches and challenges. *Advances in Water Resources*, *25*(8-12), 899–944. https://doi.org/10.1016/S0309-1708(02)00063-5

Duffy, C. J., & Al-Hassan, S. (1988). Groundwater circulation in a closed desert basin: Topographic scaling and climatic forcing. *Water Resources Research*, *24*(10), 1675–1688. https://doi.org/10.1029/WR024i010p01675

Fan, Y., Duffy, C. J., Douglas, J., & Oliver, S. (1997). Density-driven groundwater flow in closed desert basins field investigations and numerical experiments. *Journal of Hydrology*, *196*(1-4), 139–184. https://doi.org/10.1016/S0022-1694(96)03292-1

Garven, G. (1989). A hydrogeologic model for the formation of the giant oil sands deposits of the western Canada sedimentary basin. *American Journal of Science*, *289*(2), 105–166. https://doi.org/10.2475/ajs.289.2.105

Garven, G. (1995). Continental-scale groundwater flow and geologic process. *Annual Review of Earth and Planetary Sciences*, *23*, 89–117. https://doi.org/10.1146/annurev.ea.23.050195.000513

Garven, G., Appold, M. S., Toptygina, V. I., & Hazlett, T. J. (1999). Hydrogeologic modeling of the genesis of carbonate-hosted lead-zinc ores. *Hydrogeology Journal*, *7*(1), 108–126. https://doi.org/10.1007/s100400050183

Garven, G., & Freeze, R. A. (1984). Theoretical analysis of the role of groundwater flow in the genesis of stratabound ore deposits; 1, Mathematical and numerical model. *American Journal of Science*, *284*, 1085–1124.
Garven, G., Ge, S., Person, M. A., & Sverjensky, D. A. (1993). Genesis of stratabound ore deposits in the midcontinent basins of North America; 1, The role of regional groundwater flow. *American Journal of Science*, *293*, 497–568.
Geng, X., & Boufadel, M. C. (2015a). Impacts of evaporation on subsurface flow and salt accumulation in a tidally influenced beach. *Water Resources Research*, *51*, 5547–5565. https://doi.org/10.1002/2015WR016886
Geng, X., & Boufadel, M. C. (2015b). Numerical modeling of water flow and salt transport in bare saline soil subjected to evaporation. *Journal of Hydrology*, *524*, 427–438. https://doi.org/10.1016/j.jhydrol.2015.02.046
Gleeson, T., & Manning, A. H. (2008). Regional groundwater flow in mountainous terrain: Three-dimensional simulations of topographic and hydrogeologic controls. *Water Resources Research*, *44*, W10403. https://doi.org/10.1029/2008WR006848
Graf, T., & Therrien, R. (2005). Variable-density groundwater flow and solute transport in porous media containing nonuniform discrete fractures. *Advances in Water Resources*, *28*(12), 1351–1367. https://doi.org/10.1016/j.advwatres.2005.04.011
Gulley, J. D., Mayer, A. S., Martin, J. B., & Bedekar, V. (2016). Sea level rise and inundation of island interiors: Assessing impacts of lake formation and evaporation on water resources in arid climates. *Geophysical Research Letters*, *43*, 9712–9719. https://doi.org/10.1002/2016GL070667
Gupta, I., Wilson, A. M., & Rostron, B. J. (2015). Groundwater age, brine migration, and large-scale solute transport in the Alberta Basin, Canada. *Geofluids*, *15*(4), 608–620. https://doi.org/10.1111/gfl.12131
Han, D., Kohfahl, C., Song, X., Xiao, G., & Yang, J. (2011). Geochemical and isotopic evidence for palaeo-seawater intrusion into the south coast aquifer of Laizhou Bay, China. *Applied Geochemistry*, *26*(5), 863–883. https://doi.org/10.1016/j.apgeochem.2011.02.007
Jiang, X.-W., Wan, L., Cardenas, M. B., Ge, S., & Wang, X.-S. (2010). Simultaneous rejuvenation and aging of groundwater in basins due to depth-decaying hydraulic conductivity and porosity. *Geophysical Research Letters*, *37*, L05403. https://doi.org/10.1029/2010GL042387
Jiang, X.-W., Wan, L., Wang, J.-Z., Yin, B.-X., Fu, W.-X., & Lin, C.-H. (2014). Field identification of groundwater flow systems and hydraulic traps in drainage basins using a geophysical method. *Geophysical Research Letters*, *41*, 2812–2819. https://doi.org/10.1002/2014GL059579
Jiang, X.-W., Wan, L., Wang, X.-S., Ge, S., & Liu, J. (2009). Effect of exponential decay in hydraulic conductivity with depth on regional groundwater flow. *Geophysical Research Letters*, *36*, L24402. https://doi.org/10.1029/2009GL041251
Jiao, J., & Post, V. (2019). *Coastal hydrogeology*. New York: Cambridge University Press. https://doi.org/10.1017/9781139344142
Jiao, J. J., Zhang, X., & Wang, X. (2015). Satellite-based estimates of groundwater depletion in the Badain Jaran Desert, China. *Scientific Reports*, *5*, 8960. https://doi.org/10.1038/srep08960
Kohfahl, C., Post, V. E. A., Hamann, E., Prommer, H., & Simmons, C. T. (2015). Validity and slopes of the linear equation of state for natural brines in salt lake systems. *Journal of Hydrology*, *523*, 190–195. https://doi.org/10.1016/j.jhydrol.2015.01.054
Lee, M.-K., & Bethke, C. M. (1994). Groundwater flow, late cementation, and petroleum accumulation the Permian Lyons sandstone, Denver basin. *AAPG Bulletin*, *78*(2), 221–241.
Person, M., Raffensperger, J. P., Ge, S., & Garven, G. (1996). Basin-scale hydrogeologic modeling. *Reviews of Geophysics*, *34*(1), 61–87. https://doi.org/10.1029/95RG03286
Raffensperger, J. P., & Garven, G. (1995). The formation of unconformity-type uranium ore deposits; 1, Coupled groundwater flow and heat transport modeling. *American Journal of Science*, *295*, 581–636.
Rioual, P., Lu, Y., Yang, H., Scuderi, L., Chu, G., Holmes, J., et al. (2013). Diatom–environment relationships and a transfer function for conductivity in lakes of the Badain Jaran Desert, Inner Mongolia, China. *Journal of Paleolimnology*, *50*(2), 207–229. https://doi.org/10.1007/s10933-013-9715-9
Santos, I. R., Niencheski, F., Burnett, W., Peterson, R., Chanton, J., Andrade, C. F. F., et al. (2008). Tracing anthropogenically driven groundwater discharge into a coastal lagoon from southern Brazil. *Journal of Hydrology*, *353*(3-4), 275–293. https://doi.org/10.1016/j.jhydrol.2008.02.010
Schwartz, F. W., & Domenico, P. A. (1973). Simulation of hydrochemical patterns in regional groundwater flow. *Water Resources Research*, *9*(3), 707–720. https://doi.org/10.1029/WR009i003p00707
Stuyfzand, P. J. (1999). Patterns in groundwater chemistry resulting from groundwater flow. *Hydrogeology Journal*, *7*, 15–27. https://doi.org/10.1007/s100400050177
Szijártó, M., Galsa, A., Tóthb, Á., & Mádl-Szőnyi, J. (2019). Numerical investigation of the combined effect of forced and free thermal convection in synthetic groundwater basins. *Journal of Hydrology*, *572*, 364–379. https://doi.org/10.1016/j.jhydrol.2019.03.003
Therrien, R., McLaren, R. G., Sudicky, E. A., & Panday, S. M. (2006). *HydroGeoSphere: A three-dimensional numerical model describing fully-integrated subsurface and surface flow and solute transport* (p. 349). Waterloo, Ontario: Groundwater Simul. Group.
Tóth, J. (1963). A theoretical analysis of groundwater flow in small drainage basins. *Journal of Geophysical Research*, *68*(16), 4795–4812. https://doi.org/10.1029/JZ068i016p04795
Tóth, J. (1999). Groundwater as a geologic agent: An overview of the causes, processes, and manifestations. *Hydrogeology Journal*, *7*, 1–14.
Waiser, M. J., & Robarts, R. D. (2009). Saline Inland Waters. In *Encyclopedia of Inland Waters* (Vol. 2, pp. 634–644). Oxford: Elsevier.
Wang, H., Jiang, X.-W., Wan, L., Han, G., & Guo, H. (2015). Hydrogeochemical characterization of groundwater flow systems in the discharge area of a river basin. *Journal of Hydrology*, *527*, 433–441. https://doi.org/10.1016/j.jhydrol.2015.04.063
Wang, N., Ning, K., Li, Z., Wang, Y., Jia, P., & Ma, L. (2016). Holocene high lake-levels and pan-lake period on Badain Jaran Desert. *Science China Earth Sciences*, *59*(8), 1633–1641. https://doi.org/10.1007/s11430-016-5307-7
Wang, X.-S., Jiang, X.-W., Wan, L., Ge, S., & Li, H. (2011). A new analytical solution of topography-driven flow in a drainage basin with depth-dependent anisotropy of permeability. *Water Resources Research*, *47*, W09603. https://doi.org/10.1029/2011WR010507
Wang, X.-S., & Zhou, Y. (2018). Investigating the mysteries of groundwater in the Badain Jaran Desert, China. *Hydrogeology Journal*, *26*(5), 1639–1655. https://doi.org/10.1007/s10040-018-1750-1
Wang, Y., & Jiao, J. J. (2012). Origin of groundwater salinity and hydrogeochemical processes in the confined quaternary aquifer of the Pearl River Delta, China. *Journal of Hydrology*, *438-439*, 112–124. https://doi.org/10.1016/j.jhydrol.2012.03.008
Weisbrod, N., Yechieli, Y., Shandalov, S., & Lensky, N. (2016). On the viscosity of natural hyper-saline solutions and its importance: The Dead Sea brines. *Journal of Hydrology*, *532*, 46–51. https://doi.org/10.1016/j.jhydrol.2015.11.036
Werner, A. D., Bakker, M., Post, V. E. A., Vandenbohede, A., Lu, C. H., Ataie-Ashtiani, B., et al. (2013). Seawater intrusion processes, investigation and management: Recent advances and future challenges. *Advances in Water Resources*, *51*, 3–26. https://doi.org/10.1016/j.advwatres.2012.03.004
Wilson, A. M. (2005). Fresh and saline groundwater discharge to the ocean: A regional perspective. *Water Resources Research*, *41*, W02016. https://doi.org/10.1029/2004WR003399

Wooding, R. A., Tyler, S. W., & White, I. (1997). Convection in groundwater below an evaporating salt lake: 1. Onset of instability. *Water Resources Research*, *33*(6), 1199–1217. https://doi.org/10.1029/96WR03533

Yang, X. (2000). Landscape evolution and precipitation changes in the Badain Jaran Desert during the last 30000 years. *Chinese Science Bulletin*, *45*(11), 1042–1047. https://doi.org/10.1007/BF02884988

Zlotnik, V. A., Cardenas, M. B., & Toundykov, D. (2011). Effects of multiscale anisotropy on basin and hyporheic groundwater flow. *Groundwater*, *49*(4), 576–583. https://doi.org/10.1111/j.1745-6584.2010.00775.x